Japanese Journal of Radiology (2024) 42:519–535
https://doi.org/10.1007/s11604-024-01529-z

ORIGINAL ARTICLE

Combined visual and quantitative assessment of somatostatin receptor scintigraphy for staging and restaging of neuroendocrine tumors

Yuya Ueki[1] · Hideki Otsuka[2] · Tamaki Otani[3] · Ryosuke Kasai[2] · Yoichi Otomi[4] · Daiki Ikemitsu[5] · Shota Azane[5] · Yamato Kunikane[5] · Takanori Bando[5] · Noritake Matsuda[5] · Yasuyuki Okada[6] · Tetsuji Takayama[6] · Masafumi Harada[4]

Received: 11 September 2023 / Accepted: 3 January 2024 / Published online: 12 February 2024

Abstract

Purpose Somatostatin receptor scintigraphy (SRS) using ^{111}In-DTPA-DPhe^{1}-octreotide (pentetreotide) has become an integral part of neuroendocrine neoplasm management. The lack of precise quantification is a disadvantage of SRS. This study aimed to adapt the standardized uptake value (SUV) to SRS, establish the SUV range for physiological uptake in the liver, kidney, and spleen, and elucidate the utility of combined visual and quantitative SRS assessment for staging and restaging of neuroendocrine tumors (NETs).

Materials and methods This study included 21 patients with NETs who underwent ^{111}In-pentetreotide SRS. The SUV of physiological and pathological uptake was calculated using bone single-photon emission computed tomography (SPECT) quantitative analysis software (GI-BONE). For visual analysis, the primary and metastatic lesions were scored visually on planar and SPECT images using a five-point scale. We assessed the relationships between the SUVs of the liver, kidney, and spleen in the dual phase, and among quantitative indices, visual score, and pathological lesions classification.

Results Sixty-three NEN lesions were evaluated. The mean ± standard deviation maximum SUVs (SUVmax) were liver: 4 h, 2.6 ± 1.0; 24 h, 2.2 ± 1.0; kidney: 4 h, 8.9 ± 1.8; 24 h, 7.0 ± 2.0; and spleen; 4 h, 11.3 ± 4.5; 24 h, 11.5 ± 7.6. Higher SUVmax was significantly associated with higher visual scores on dual-phase SPECT (4 h, $p < 0.001$; 24 h, $p < 0.001$) (4 h: scores 3 and 4, $p < 0.05$; scores 3 and 5: $p < 0.01$; scores 4 and 5: $p < 0.01$; 24 h: scores 3 and 4, $p = 0.0748$; scores 3 and 5: $p < 0.01$; scores 4 and 5: $p < 0.01$).

Conclusion We adapted the SUV to SRS and established the range of SUV for physiological uptake in the liver, kidney, and spleen. Combined visual and quantitative assessment is useful for imaging individual lesions in greater detail, and may serve as a new tumor marker of SRS for staging and restaging of NETs.

Keywords ^{111}In-pentetreotide · Somatostatin receptor (SSTR) · Somatostatin receptor scintigraphy (SRS) · Neuroendocrine tumors (NETs) · Becquerel calibration factor (BCF) · Standardized uptake value (SUV)

✉ Hideki Otsuka
hideki.otsuka@tokushima-u.ac.jp

[1] Tokushima University Graduate School of Health Sciences, Tokushima, Japan

[2] Department of Medical Imaging/Nuclear Medicine, Tokushima University Graduate School of Biomedical Sciences, Tokushima, Japan

[3] Advance Radiation Research, Education and Management Center, Tokushima University, Tokushima, Japan

[4] Department of Radiology and Radiation Oncology, Tokushima University Graduate School of Biomedical Sciences, Tokushima, Japan

[5] Department of Radiology, Tokushima University Hospital, Tokushima, Japan

[6] Department of Gastroenterology and Oncology, Tokushima University Graduate School of Biomedical Sciences, Tokushima, Japan

Introduction

Neuroendocrine neoplasms (NENs) are rare tumors arising from neuroendocrine cells present throughout the body, mainly in the pancreas and gastrointestinal tract; however, their incidence has risen due to an increase in early diagnoses, with stage migration potentially also playing a role [1, 2]. The 2019 World Health Organization (WHO) classification categorizes NENs as neuroendocrine tumors (NETs) and neuroendocrine carcinomas (NECs). NETs are further classified into three subgroups, grades 1, 2, and 3, according to pathological differentiation, grade, and proliferative activity.

Morphologic imaging modalities, including computed tomography (CT), magnetic resonance imaging, ultrasonography, and nuclear medicine imaging, are widely used in NET management [3]. Nuclear imaging enables visualization of the somatostatin receptor (SSTR) expressed on tumor cells using radionuclide-labeled SSTR analogs that bind specifically to the tumor cells, resulting in SSTR imaging. Since its advent in the 1980s, SSTR imaging has evolved from single photon radioisotope scintigraphy (somatostatin receptor scintigraphy [SRS]) to ^{111}In-DTPA-DPhe1-octreotide (pentetreotide) SRS and ^{68}Ga-positron emission tomography (PET) in the 2010s. SSTR imaging, including peptide receptor radionuclide therapy (PRRT), has been adopted in the management of patients with NENs for staging, restaging, and follow-up to localize the primary tumor, metastases, and recurrence and to monitor the reaction to treatment [4]. A major difference between SRS and PET is that the latter enables quantitative analysis [5]. Lesion uptake in SRS is assessed using visual scores, with the physiological uptake by the liver, kidney, and spleen as the standard [6]. However, the lack of precise quantification is a disadvantage of SRS. To date, there are no reports on evaluating SRS using quantitative indices. PET, which yields high-quality images, can estimate tracer uptake as a quantitative parameter, the standardized uptake value (SUV). Generally, PET offers superior quantitative analysis over SRS; moreover, quantitative analysis software for single-photon emission computed tomography (SPECT) has been developed for clinical use [7, 8].

Therefore, this study aimed to adapt the SUV to SRS, to establish the SUV range of physiological uptake in the liver, kidney, and spleen, to clarify the relationship between conventionally used visual assessment and quantitative indices using SUV, and evaluate the utility of quantitative assessment for SR activity at staging and determining treatment efficacy, including PRRT at restaging of NETs.

Materials and methods

This retrospective study was approved by the research ethics committee of Tokushima University Hospital, which waived the requirement for written informed consent. The information disclosure document for this study is available to the public on Tokushima University Hospital's website. We performed phantom and clinical studies using a hybrid SPECT/CT system (Symbia T16; Siemens, Germany).

Phantom study

We conducted a phantom experiment to calculate the Becquerel calibration factor (BCF) for converting the count scale of SPECT to the radiation dose. A cylindrical phantom (inner diameter: 16 cm, length: 15 cm, and volume: 3016 mL; Sangyo Kagaku, Tokyo, Japan) was encapsulated with water and 24.6 MBq of ^{111}In-DTPA. The phantom experiment entailed performing SPECT imaging for 15 min, and the data were reconstructed according to the clinical ^{111}In-pentetreotide SPECT/CT protocol (Table 1). We acquired the BCF of ^{111}In using the bone SPECT analysis software, GI-BONE (AZE Corp., Tokyo, Japan), to calculate the SUV.

Patient study

The patient characteristics, primary site, and pathological grade are presented in Table 2. This study included 29 examinations of 21 patients (12 men, 9 women; age 37–83 years) who underwent SRS with ^{111}In-pentetreotide

Table 1 Image processing

SPECT/CT scanner	Symbia T16 (Siemens)
RI	^{111}In
Collimator	LMEGP
keV	158–183 keV, 227–263 keV
Matrix	128 × 128
Pixel size	3.9 mm
Imaging processing	Continuous mode
Rotation	180°
Collection time	30 s × 30
Attenuation correction	CTAC
Filter	
OSEM	Gaussian 10.00 mm
OSEM	
Subset number	6
Iterations	12

SPECT single-photon emission computed tomography, *CT* computed tomography

Table 2 Patient characteristics

	Grade	Total	Initial staging	Follow-up
Number of patients (examinations)		21 (29)	15 (15)	6 (14)
Men/women		12/9	8/7	4/2
Age: mean (range)		62.3 (37–83)	65.3 (37–83)	59.1 (47–77)
Body weight: mean (SD)		62.3 (17.6)	61.8 (14.0)	62.8 (21.4)
Pancreas	1	1	1	
	2	6	3	3
	Unknown	5	5	
Duodenum	2	4	2	2
Lung	2	2	1	1
Pancreatic duodenum	1	1	1	
Rectum	1	1	1	
Unknown	2	1	1	

SD standard deviation

at Tokushima University Hospital between June 2016 and March 2023. We examined 15 SRS scans of 15 treatment-naive patients who underwent a single SRS session for initial staging and 14 SRS scans of 6 patients (three scans each of two patients and two scans each of four patients) who underwent repeated SRS examinations for follow-up; there was no overlap between the patients who underwent initial staging and those who underwent follow-up examinations. The clinical diagnosis was confirmed by board-certified gastroenterologists. Pathological confirmation was performed in 16 patients with the following results: 7 pancreatic NETs (P-NET), 4 duodenal NETs (D-NET), 2 lung NETs, 1 rectal NET, 1 pancreaticoduodenal NET, and 1 NET of unknown primary site. Dual-phase whole-body planar imaging and SPECT/CT were performed approximately 4 h and 24 h after intravenous injection of 111 MBq of ^{111}In-pentetreotide. CT data were used for attenuation correction and to obtain anatomical information. The body weight and injected radiation dose were recorded for all patients and used to calculate the SUV.

Visual evaluation

All lesions were independently scored on both planar and SPECT images by two board-certified nuclear medicine specialists. Anterior- and posterior-view planar images were examined using a diagnostic viewer system (Centricity Universal Viewer; GE Healthcare) and SPECT/CT images (three types of images, viz, SPECT, CT, and SPECT/CT; thickness: 2 mm in the three-dimensional axial, coronal, and sagittal views) were examined using the AquariousNET workstation (TeraRecon, Inc.) on separate days. All images were displayed on a RadiForce RX270 21.3 Color LCD Monitor (EIZO Co.). In cases of discrepancy between the findings, the final score was determined via discussion. In cases of multiple lesions, the lesion with the most intense uptake was included in the analysis. The lesion accumulation was compared with the background, liver, and kidney accumulation and scored according to the scoring system shown below. The uptake in the liver and kidneys was comprehensively evaluated using both planar and SPECT/CT images; the uptake in the entire organ was evaluated, especially for the kidney, owing to its heterogeneous structure.

Visual score 1: ≤ Background
Visual score 2: Background < Lesion < Liver
Visual score 3: = Liver
Visual score 4: Liver < Lesion < Kidney
Visual score 5: ≤ Kidney

Quantitative assessment

SUV

The radiation count was converted to a measure of the radioactivity using the BCF as follows: radioactivity of the region (Bq) = (radiation count of the region) × BCF. The bone SPECT analysis software, GI-BONE (AZE Corp., Tokyo, Japan), was used to calculate the SUV using the following formula: SUV = mean volume of interest (VOI) activity (MBq/g)/[injected dose (MBq)/body weight (g)] = [(total count of the VOI) × BCF/volume of VOI]/[injected dose/body weight].

Physiological uptake on SPECT

The maximum (SUVmax), peak (SUVpeak), and mean (SUVmean) SUVs of physiological uptake in the liver, kidney, and spleen were calculated in the dual phase during initial staging in 15 patients (Fig. 1). No threshold was set for the VOI. The VOI was set only for the liver, kidney, and spleen, respectively, so the surrounding organs were not included and confirmed in the three dimensions of the

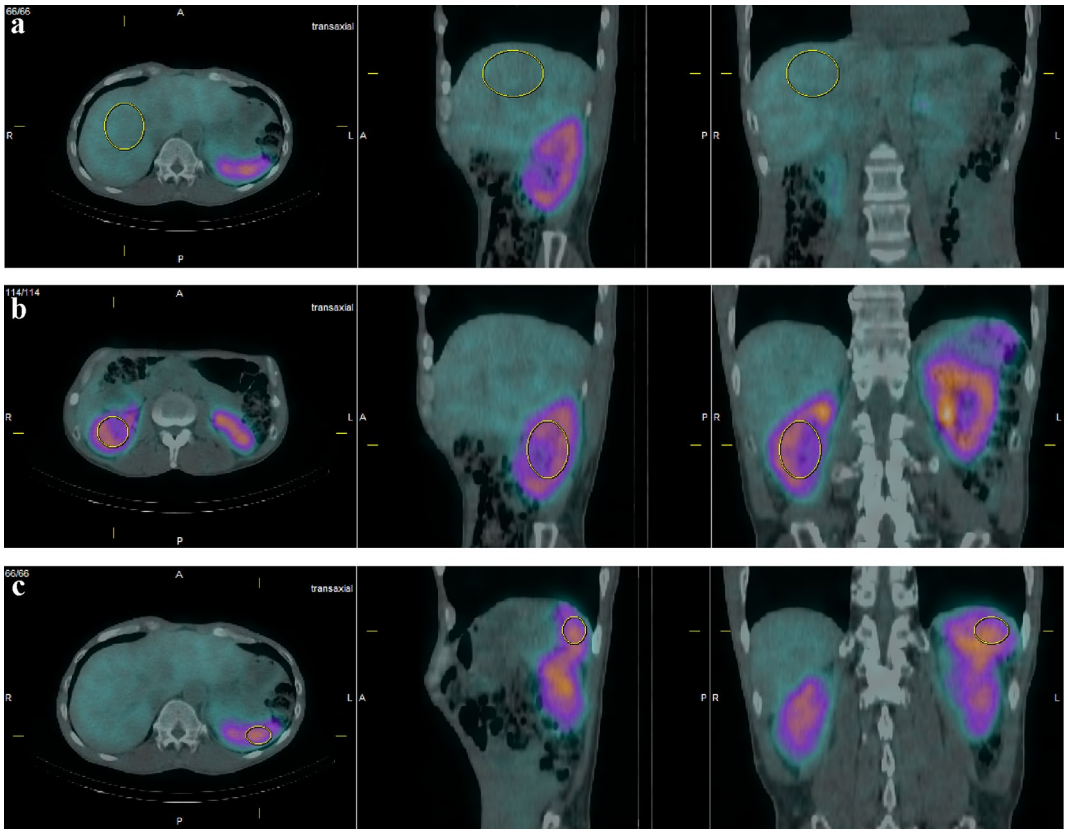

Fig. 1 VOI image on GI-BONE showing physiological uptake. VOI image: **a** liver, **b** kidney, **c** spleen. Each VOI is set in a three-dimensional plane. *VOI* volume of interest

horizontal, coronal, and sagittal views. Four patients with liver metastasis were excluded from the liver analysis.

Lesion uptake

The SUVmax of the primary lesion, liver, lymph node, and bone metastasis in the dual phase were measured separately using the previous BCF. In cases of multiple liver, lymph nodes, and bone lesions, the lesion with the highest uptake intensity was included in the analysis. All lesions were assessed to investigate the relationship between visual scoring and quantitative analysis, and the SUVmax and visual scores of 15 primary lesions in the initial staging group were compared with the WHO pathological classification. Figure 2 depicts the images of a patient with a grade 2 primary D-NET measuring 2.3 cm, which showed homogeneous enhancement and multiple liver metastases with lower density than that of the liver parenchyma.

Treatment response

To evaluate the treatment response, we calculated the reduction score and reduction rate as follows:

$$\text{Reduction score} = (\text{preVisual score}) - (\text{postVisual score})$$

$$\text{Reduction rate}\ (\%) = \left\{\left[(\text{preSUVmax}) - (\text{postSUVmax})\right]/\text{preSUVmax}\right\} \times 100$$

Statistical analysis

Wilcoxon's signed-rank test was used to compare the physiological uptake of each organ in the respective phase. Based on the histograms and quantile–quantile plots, a non-parametric distribution of SUVmax (i.e., lesion uptake) was assumed.

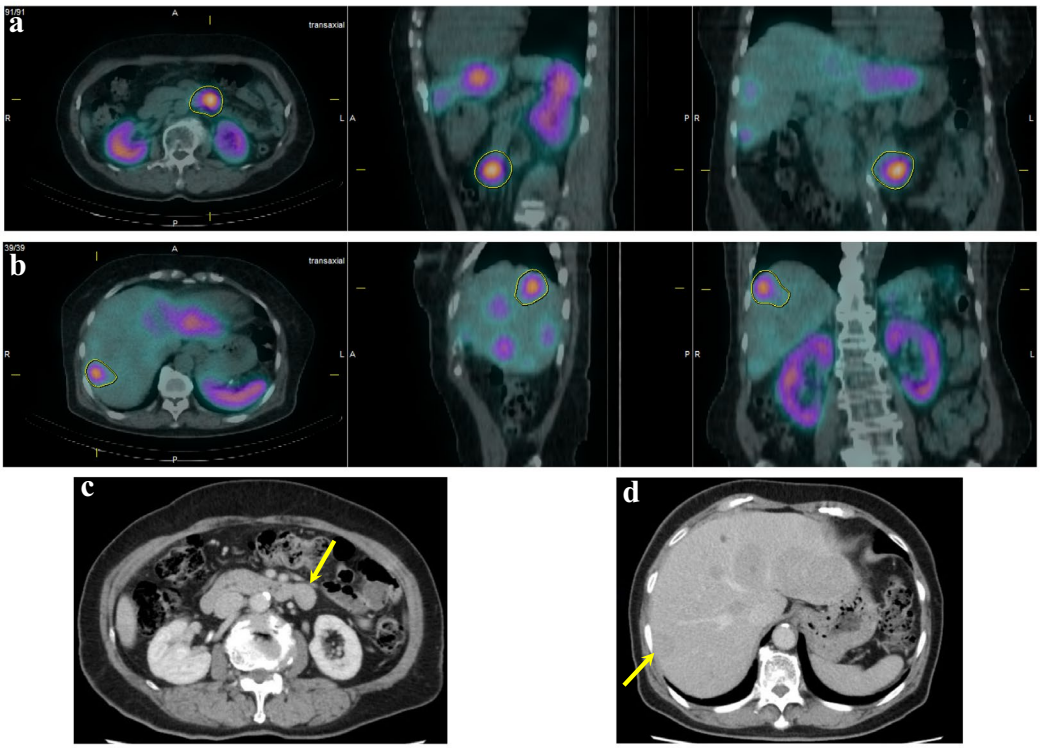

Fig. 2 NET of the duodenum. VOI image: **a** primary lesion, **b** liver metastasis. Contrast-enhanced CT in the delayed phase, **c** primary lesion, **d** liver metastasis. NET of the duodenum, measuring 2.3 cm, shows homogeneous enhancement and multiple liver metastases with low density compared with that of the liver parenchyma. *NET* neuroendocrine tumor, *CT* computed tomography

The association between lesion uptake measured as the SUVmax and the visual score on SPECT was compared using the Kruskal–Wallis test and Steel–Dwass test for unpaired data. Statistical significance was set at $p < 0.05$. All statistical analyses were performed using Bellcurve for Excel, version 4.04.

Results

Phantom study

The BCF derived from the phantom experiment was 2195.02 Bq/cps.

Physiological uptake

The SUV of physiological uptake in patients who underwent initial staging is presented in Table 3 and Fig. 3. The mean ± standard deviation (SD) (range) of SUVmax of the liver were 2.6 ± 1.0 (1.4–4.9) and 2.2 ± 1.0 (1.1–4.6), those of the kidney were 8.9 ± 1.8 (5.4–11.5) and 7.0 ± 2.0 (3.8–11.3), and those of the spleen were 11.3 ± 4.5 (5.6–22.1) and 11.5 ± 7.6 (4.6–28.6) at 4 h and 24 h, respectively. The mean ± SD (range) of SUVpeak of the liver were 2.4 ± 1.0 (1.3–4.7) and 2.1 ± 1.0 (1.0–4.5), those of the kidney were 8.2 ± 1.7 (5.2–10.8) and 6.5 ± 1.9 (3.6–10.5), and those of the spleen were 10.7 ± 4.3 (5.4–21.0) and 10.9 ± 7.3 (4.2–28.0) at 4 h and 24 h, respectively. The mean ± SD (range) of SUVmean of the liver were 1.8 ± 0.8 (0.9–3.8) and 1.5 ± 0.8 (0.7–3.4), those of the kidney were 5.6 ± 1.0 (3.7–7.9) and 4.3 ± 1.0 (2.3–6.0), and those of the spleen were 8.1 ± 2.5 (3.4–12.6) and 7.8 ± 3.9 (3.7–16.1) at 4 h and 24 h, respectively.

Four patients with liver metastases and one with one kidney were excluded from the liver and kidney analyses, respectively. There were no significant differences in the SUV indices of the spleen after 4 h and 24 h (Wilcoxon's signed-rank, SUVmax; $p = 0.1914$, SUVpeak; $p = 0.1914$, SUVmean; $p = 0.1252$), but there were significant differences in the respective values corresponding to the other organs.

Combined visual and quantitative assessment

The combined visual and quantitative assessment findings of all primary and metastatic lesions are shown in Tables 4 and 5 and Fig. 4. The SUVmax increased with an increase in the visual score. The SUVmax range showed a wide variation for the visual score of 5. Moreover, the differences

Table 3 SUV of physiological uptake in patients who underwent initial staging

	NET location	Grade	Phase	SUVmax			SUVpeak			SUVmean		
				Liver	Kidney	Spleen	Liver	Kidney	Spleen	Liver	Kidney	Spleen
1	Pancreatic duodenum	1	4 h	2.0	8.1	6.5	1.8	7.5	6.1	1.3	5.1	5.3
			24 h	1.7	5.6	4.6	1.5	5.1	4.2	1.0	3.5	3.7
2	Pancreas	1	4 h	1.8	5.4	5.6	1.7	5.2	5.4	1.3	3.7	3.4
			24 h	1.5	3.8	5.2	1.3	3.6	5.1	0.9	2.3	3.9
3	Pancreas	2	4 h	2.6	9.6	9.8	2.5	9.2	9.3	1.9	7.9	8.1
			24 h	2.1	8.4	9.5	2.0	8.0	8.9	1.5	6.0	7.4
4	Pancreas	2	4 h	2.1	11.5	15.5	2.0	10.8	14.6	1.5	7.0	12.5
			24 h	1.7	7.8	14.5	1.5	7.2	13.4	1.1	4.9	11.4
5	Pancreas	2	4 h	4.9	11.0	22.1	4.7	10.0	21.0	3.8	5.8	11.5
			24 h	4.6	11.3	27.6	4.5	10.5	26.2	3.4	5.3	14.2
6	Pancreas	Unknown	4 h	2.9	8.7	8.3	2.6	7.7	7.8	2.0	5.1	6.3
			24 h	2.3	7.7	7.1	2.2	7.3	6.9	1.8	4.6	5.5
7	Pancreas	Unknown	4 h	2.4	8.7	9.7	2.2	7.8	8.7	1.5	4.8	7.2
			24 h	1.9	6.9	7.3	1.7	5.9	6.5	1.1	3.5	5.7
8	Pancreas	Unknown	4 h	2.4	9.7	10.1	2.1	9.0	9.4	1.6	6.5	7.4
			24 h	1.9	6.1	8.4	1.8	5.8	8.0	1.3	4.6	6.4
9	Pancreas	Unknown	4 h	2.4	7.3	9.3	2.3	6.8	8.6	1.6	5.2	7.6
			24 h	2.0	5.8	8.1	1.8	5.3	7.5	1.2	3.7	6.0
10	Pancreas	Unknown	4 h	4.0	10.0	16.5	3.7	9.1	15.1	2.7	5.6	12.6
			24 h	3.7	8.4	17.9	3.4	7.3	16.3	2.5	4.5	12.9
11	Duodenum	2	4 h		6.7	8.6		6.3	8.1		5.2	7.3
			24 h		5.9	6.3		5.5	5.9		4.3	5.2
12	Duodenum	2	4 h		9.5	9.8		8.9	9.3		5.8	7.1
			24 h		7.3	9.1		6.8	8.7		4.5	6.8
13	Rectum	1	4 h	1.4	6.8	9.3	1.3	6.4	8.9	0.9	4.9	7.0
			24 h	1.1	4.1	7.4	1.0	3.7	6.8	0.7	2.7	5.6
14	Unknown	2	4 h		11.2	11.8		10.3	11.3		6.4	8.7
			24 h		9.2	11.3		8.6	10.8		5.2	5.8
15	Lung	2	4 h			17.2			16.5			9.4
			24 h			28.6			28.0			16.1
	Total (mean ± SD)		4 h	2.6 ± 1.0	8.9 ± 1.8	11.3 ± 4.5	2.4 ± 1.0	8.2 ± 1.7	10.7 ± 4.3	1.8 ± 0.8	5.6 ± 1.0	8.1 ± 2.5
			24 h	2.2 ± 1.0	7.0 ± 2.0	11.5 ± 7.6	2.1 ± 1.0	6.5 ± 1.9	10.9 ± 7.3	1.5 ± 0.8	4.3 ± 1.0	7.8 ± 3.9

SUV standardized uptake value, *NET* neuroendocrine tumor, *SUVmax* maximum standardized uptake value, *SUVpeak* peak standardized uptake value, *SUVmean* mean standardized uptake value, *SD* standard deviation

between scores 3 and 4 and between scores 4 and 5 were statistically significant. The results of the combined visual and quantitative assessment with the WHO classification of patients who underwent initial staging are shown in Table 4 and Fig. 5. Sixty-three NEN lesions (primary lesion, $n = 29$; liver metastasis, $n = 18$; lymph node metastasis, $n = 11$; bone metastasis, $n = 5$) were observed. In cases of multiple lesions, the highest uptake of each site was analyzed. Visual evaluation showed that physiological uptake in the urinary system (kidneys and bladder), spleen, and highly concentrated metastases overlapped with the uptake of the lesions more frequently on planar imaging than on SPECT imaging. Additionally, since SPECT is more sensitive and accurate than planar imaging [9], the visual score was representative of these aspects of SPECT. For all NEN lesions, the correlation between the SPECT-derived visual score and SUVmax of each phase is shown in Fig. 4. A higher SUVmax was significantly associated with a higher visual score (Kruskal–Wallis: 4 h, average rank: score 3, 9.50; score 4, 22.21; score 5, 45.00; $p < 0.001$; 24 h, average rank: score 3, 9.86; score 4, 21.58; and score 5, 43.71; $p < 0.001$). Visual scores 4 and 5 showed significant differences in SUVmax at each time point (Steel–Dwass, 4 h: score 3 and score 4, $p < 0.05$; score 3 and score 5, $p < 0.01$; score 4 and score 5, $p < 0.01$; 24 h: score 3 and score 4, $p = 0.0748$; score 3 and score 5, $p < 0.01$; score 4 and score 5, $p < 0.01$). Figure 5

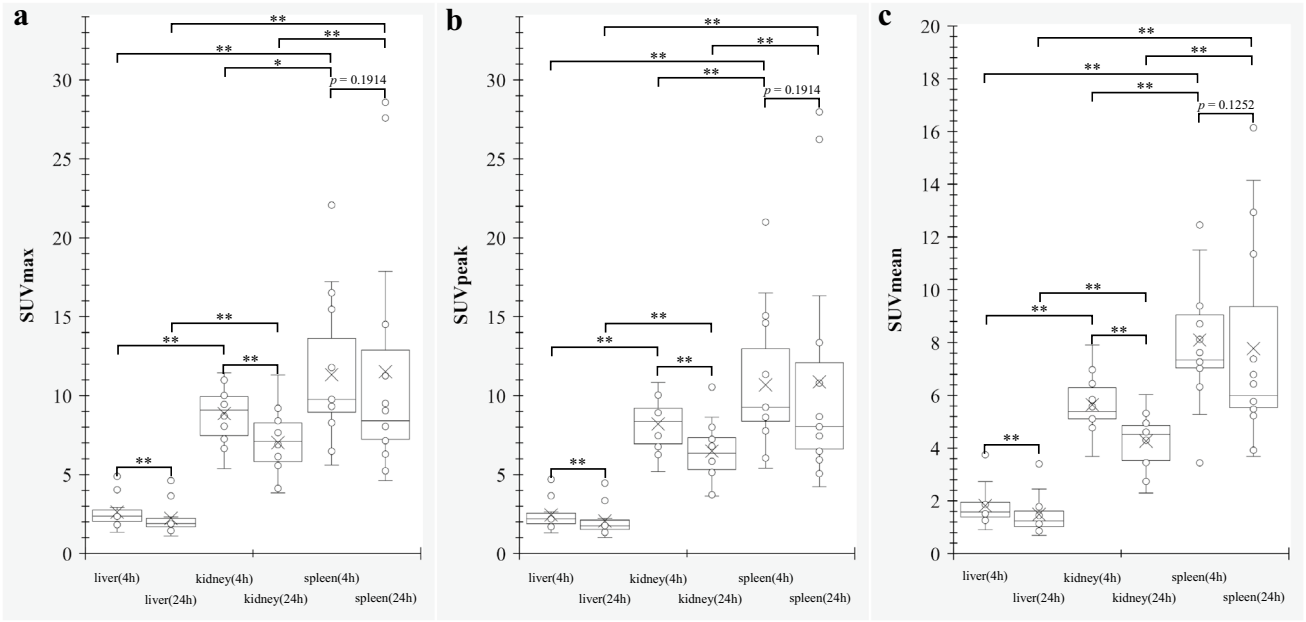

Fig. 3 Box plot analysis of physiological uptake. **a** SUVmax, **b** SUVpeak, and **c** SUVmean of the organ on dual-phase imaging (Wilcoxon signed-rank, **; $p<0.01$, *; $p<0.05$). *SUVmax* maximum standardized uptake value, *SUVpeak* peak standardized uptake value, *SUVmean* mean standardized uptake value

depicts the relationship between the WHO classification and SUVmax and that between the WHO classification and visual score on SPECT in each phase for the primary lesions of 15 patients who underwent initial imaging. All three sites diagnosed with grade 1 NET were biased towards a visual score of 5 in each phase. In contrast, grade 2 lesions showed a wider distribution for SUVmax and the visual score than grade 1 lesions. From the early to late phases, the accumulation decreased slightly in grade 1 lesions, whereas it increased, was almost unchanged, or decreased in grade 2 lesions. In contrast, only 1 out of 10 lesions showed a change in the visual score. The visual score remained constant even when the SUVmax fluctuated greatly, such as in Patients 5 and 11. Figure 6 depicts the findings of Patient 2 from the initial staging group, who had a grade 1 P-NET measuring 1.7 cm, which exhibited strong homogeneous enhancement on early-phase dynamic CT. There was no evidence of lymph node and distant metastases on body CT and SRS. The primary lesion showed intense SRS uptake, a score of 5, and an SUVmax of 5.0 in the early phase; a visual score of 5 and an SUVmax of 2.5 in the delayed phase; and an SUVmax of 1.9 on ^{18}F-fluorodeoxyglucose (FDG)-PET/CT, which closely approximated that of the pancreas. Figure 7 shows the findings of Patient 3 from the initial staging group, who had a grade 2 P-NET in the pancreatic head measuring 1.7 cm, which exhibited strong homogeneous enhancement in the early phase of dynamic CT. There was no evidence of lymph node and distant metastases on body CT and SRS. In the early phase, the primary lesion showed moderate uptake, a visual score of 3, and an SUV max of 3.4. In the delayed phase, the visual score was 4, and SUVmax was 2.5. The lesion showed intense FDG uptake with an SUVmax of 57.3 on FDG-PET/CT.

The reduction score and reduction rate of the primary and distant metastases of the patients in the follow-up group are shown in Table 6. Even when the reduction score was 0, and there was no visually apparent change in aggregation, the reduction rate ranged from − 216% to 61% after 4 h and from − 266% to 70% after 24 h. Additionally, the reduction rate after PRRT was more than 40% in all lesions in three patients, enabling quantitative evaluation of the treatment effect. Figure 8 depicts the findings of Patient 1 from the follow-up group, who had a grade 2 P-NET with liver metastasis that was treated with chemotherapy and PRRT. After the first chemotherapy course, the primary lesion at the pancreatic tail showed very intense uptake, a visual score of 5, and an SUVmax of 26.8, and the liver metastasis showed almost the same uptake as the liver, a visual score of 3, and an SUVmax of 2.5. After the second chemotherapy course, the primary lesion uptake on SRS decreased, the visual score was 5, SUVmax was 11.3, reduction score was 0, and reduction rate was 58%. Multiple liver metastases were identified, with a score of 5, an SUVmax of 19.5, a reduction score of − 2, and a reduction rate of − 691%. After PRRT, the primary lesion uptake on SRS slightly decreased compared with that on the previous scan, the visual score

Table 4 Visual score and SUVmax of primary and metastatic lesions of patients who underwent initial staging

	NET location	Grade	Phase	Primary lesion			Liver metastasis			Bone metastasis		
				Visual score		SUVmax	Visual score		SUVmax	Visual score		SUVmax
				Planar	SPECT		Planar	SPECT		Planar	SPECT	
1	Pancreatic duodenum	1	4 h	3	5	8.0						
			24 h	4	5	5.2						
2	Pancreas	1	4 h	5	5	5.0						
			24 h	5	5	2.5						
3	Pancreas	2	4 h	2	3	3.4						
			24 h	2	4	2.5						
4	Pancreas	2	4 h	5	4	6.6						
			24 h	4	4	4.4						
5	Pancreas	2	4 h	5	5	34.0						
			24 h	5	5	44.8						
6	Pancreas	Unknown	4 h	2	3	2.9						
			24 h	2	3	2.1						
7	Pancreas	Unknown	4 h	2	3	3.1						
			24 h	2	4	3.7						
8	Pancreas	Unknown	4 h	2	4	2.9						
			24 h	2	4	1.8						
9	Pancreas	Unknown	4 h	n/a	4	5.7						
			24 h	n/a	5	4.8						
10	Pancreas	Unknown	4 h	n/a	5	14.2						
			24 h	n/a	5	14.9						
11	Duodenum	2	4 h	5	5	25.4	4	4	5.1			
			24 h	5	5	19.6	4	4	2.5			
12	Duodenum	2	4 h	5	5	11.4	5	5	9.7			
			24 h	5	5	10.8	5	5	6.8			
13	Rectum	1	4 h	5	5	10.3						
			24 h	5	5	9.1						
14	Unknown	2	4 h	3	3	4.3	5	5	11.7	3	4	6.9
			24 h	3	3	3.0	5	5	11.6	3	4	5.5
15	Lung	2	4 h	3	3	3.3	4	4	8.5			
			24 h	3	3	4.5	4	4	13.3			

SUVmax maximum standardized uptake value, *NET* neuroendocrine tumor, *SPECT* single-photon emission computed tomography, *n/a* not applicable

was 4, SUVmax was 4.6, reduction score was 1, and reduction rate was 59%. Multiple liver metastases were observed, with a score of 4, an SUVmax of 4.0, a reduction score of 1, and a reduction rate of 80%. The pattern and degree of physiological uptake of the liver, kidney, and spleen varied among individuals. The liver, spleen, and kidneys showed high accumulation after the first chemotherapy course. The liver and kidneys showed almost equal accumulation, which was higher than that of the spleen, after the second chemotherapy course. In contrast, the spleen showed higher accumulation than the kidneys after PRRT.

Discussion

We first adapted the SUV to SRS, established the SUV range of physiological uptake in the liver, kidney, and spleen, clarified the relationship between conventional visual analysis and quantitative indices using SUV, and demonstrated the utility of quantitative assessment for SR activity at staging and for evaluation of treatment response, including PRRT at restaging of NETs.

Nuclear imaging, such as SPECT and PET, plays a vital role in managing patients with NEN. SSTR imaging with ^{111}In-pentetreotide or ^{68}Ga-labeled PET can enable visualization of SSTR expression and is useful for grade 1 and 2 NETs. FDG-PET can be used to visualize tumor activity

Table 5 Visual score and SUVmax of primary and metastatic lesions of patients who underwent follow-up

	NET location	Grade	Therapy	Phase	Primary lesion			Liver metastasis			Lymph node metastasis			Bone metastasis		
					Visual score		SUVmax	Visual score		SUVmax	Visual score		SUVmax	Visual score		SUVmax
					Planar	SPECT		Planar	SPECT		Planar	SPECT		Planar	SPECT	
1	Pancreas	2	Chemo	4 h	5	5	26.8	n/a	3	2.5						
				24 h	5	5	17.6	n/a	3	1.9						
			Chemo	4 h	4	5	11.3	5	5	19.5						
				24 h	4	5	8.8	5	5	16.8						
			PRRT	4 h	4	4	4.6	4	4	4.0						
				24 h	4	4	3.3	4	4	3.4						
2	Pancreas	2	Chemo	4 h	5	5	32.6	5	5	23.3	5	5	54.7			
				24 h	5	5	21.8	5	5	15.7	5	5	39.9			
			Chemo	4 h	5	5	51.9	5	5	66.4	5	5	59.9			
				24 h	5	5	42.5	5	5	57.6	5	5	50.4			
			PRRT	4 h	n/a	2	2.2	3	4	4.2	n/a	n/a	2.2			
				24 h	n/a	2	2.1	3	4	3.0	n/a	n/a	1.5			
3	Pancreas	2	Chemo	4 h	5	5	17.4	4	4	5.5	n/a	5	13.3			
				24 h	5	5	17.1	4	4	5.2	n/a	5	14.5			
			Chemo	4 h	5	5	19.6	5	5	12.1	n/a	5	22.0			
				24 h	5	5	27.0	5	5	13.6	n/a	5	31.1			
4	Duodenum	2	Chemo	4 h	n/a	4	3.9	4	4	6.0	4	5	10.2	5	5	9.0
				24 h	n/a	4	3.4	4	4	4.7	4	5	9.2	5	5	6.8
			Chemo	4 h	n/a	4	7.2	4	4	18.9	4	5	12.3	5	5	6.1
				24 h	n/a	4	5.5	4	4	16.3	4	5	10.3	5	5	4.7
5	Duodenum	2	Chemo	4 h	5	5	20.1	4	4	6.7	4	4	2.6			
				24 h	5	5	11.9	4	4	5.6	4	4	1.3			
			Chemo	4 h	5	5	22.1	4	4	7.3	4	4	2.6			
				24 h	5	5	19.1	4	4	7.2	4	4	2.0			
6	Lung	2	Chemo	4 h	4	5	6.5	5	5	14.8	3	3	2.1	4	4	3.1
				24 h	4	5	5.9	5	5	15.0	3	3	2.1	4	4	2.6
			PRRT	4 h	3	3	3.2	5	5	5.8	1	1	1.2	3	3	1.2
				24 h	3	3	1.9	5	5	4.5	1	2	0.5	3	3	0.6

SUVmax maximum standardized uptake value, *NET* neuroendocrine tumor, *SPECT* single-photon emission computed tomography, *Chemo* chemotherapy, *PRRT* peptide receptor radionuclide therapy, *n/a* not applicable

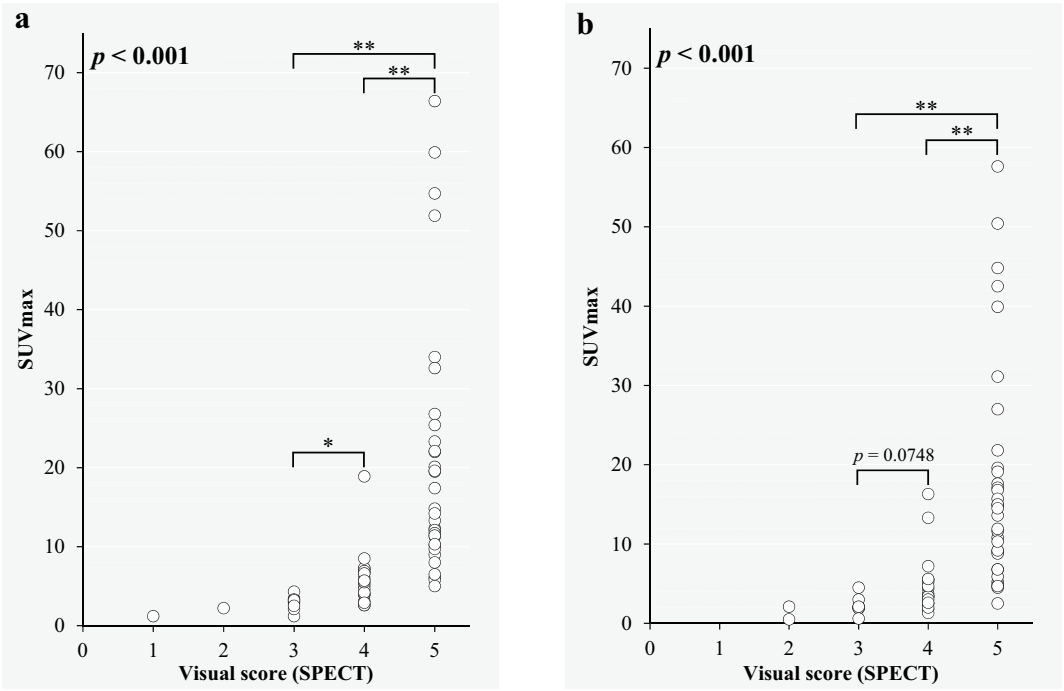

Fig. 4 Scatter plot of the relationship of the visual score on SPECT performed at **a** 4 h and **b** 24 h after injection with SUVmax (Kruskal–Wallis, $p<0.001$: Steel–Dwass, $^{**}p<0.01$, $^{*}p<0.05$). *SPECT* single-photon emission computed tomography, *SUVmax* maximum standardized uptake value

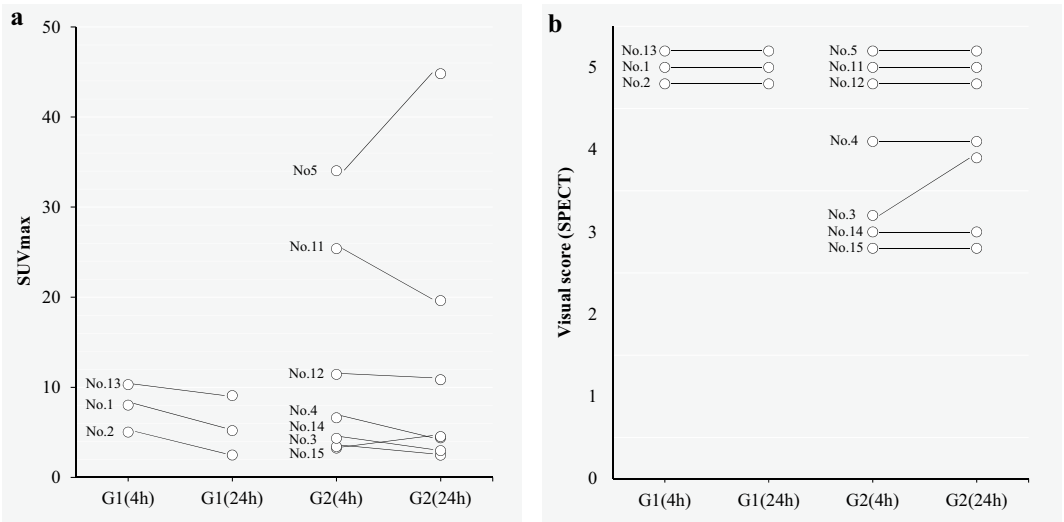

Fig. 5 **a** Scatter plot of the WHO classification in 15 patients who underwent initial staging and the SUVmax of their primary lesions, and **b** the WHO classification in 15 patients who underwent initial staging and their visual scores on SPECT. *WHO* World Health Organization, *SUVmax* maximum standardized uptake value, *SPECT* single-photon emission computed tomography

in the form of glucose metabolism and for imaging high-grade NETs and NECs. The uptake of SRS and FDG-PET is inversely correlated with pathological differentiation and tumor cell proliferation [10, 11]. To interpret SRS findings, we simultaneously assess the degree of lesion uptake in planar and SPECT/CT images. Visual scoring involves evaluating the lesion uptake with the liver, kidney, and spleen as reference. Visual scoring is simple but subjective, and the score is affected by the reference organ uptake, especially when the kidney is the reference, as the uptake pattern differs between the renal cortex and medulla. The coincidence rate and reproducibility of visual scoring are relatively

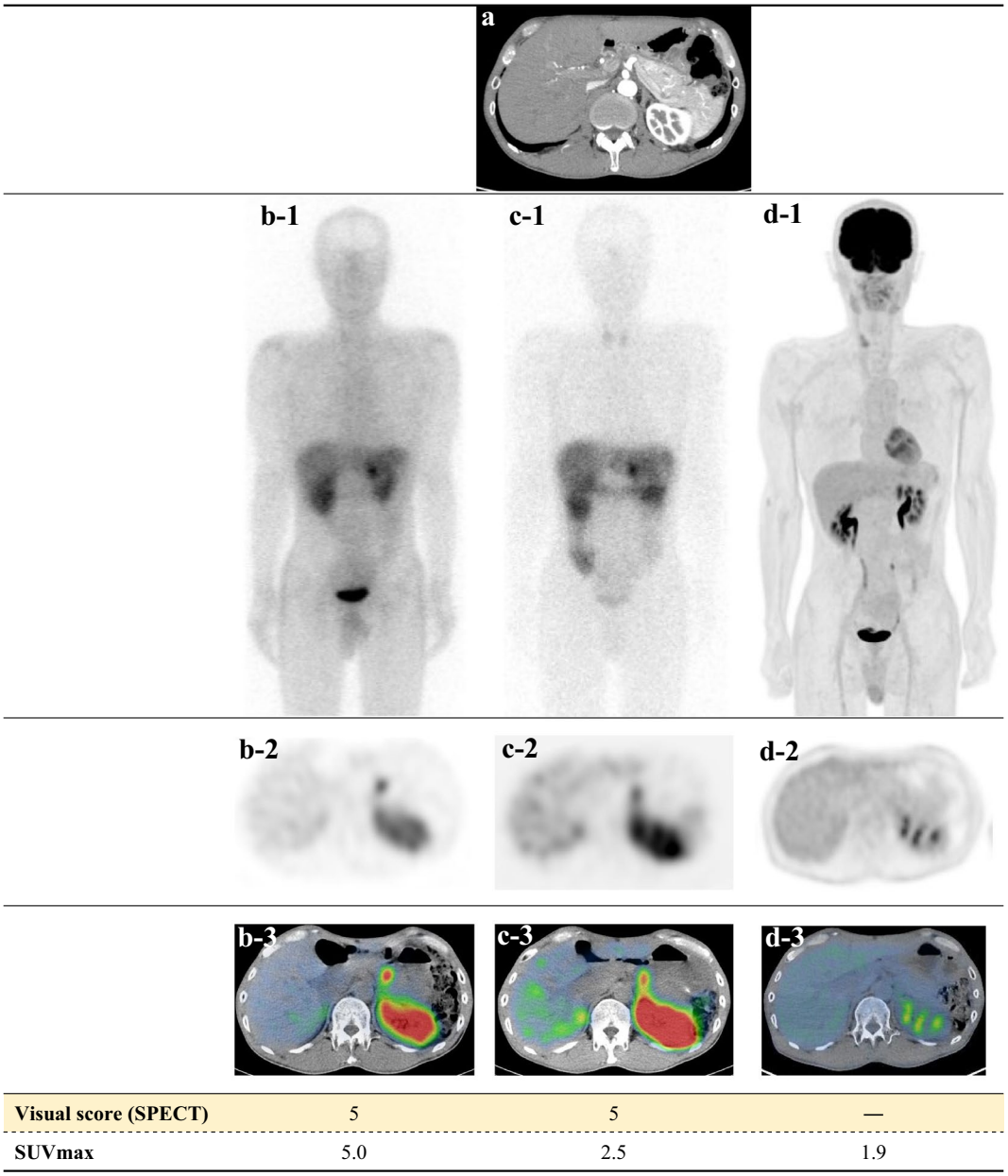

Visual score (SPECT)	5	5	—
SUVmax	5.0	2.5	1.9

Fig. 6 **a** Imaging findings of Patient 2 from the initial staging group. A grade 1 NET in the pancreas, measuring 1.7 cm, shows strong homogeneous enhancement in the early phase of dynamic CT. There is no evidence of lymph node or distant metastases on body CT and SRS. The primary lesion shows intense SRS uptake as follows: b-1 to b-3) score: 5, SUVmax: 5.0 in the early phase, c-1 to c-3) score: 5, SUVmax: 2.5 in the delayed phase, d-1 to d-3) SUVmax: 1.9 on FDG-PET/CT, approximately equal to that of the pancreas. *NET* neuroendocrine tumor, *CT* computed tomography, *SRS* somatostatin receptor scintigraphy, SUVmax: maximum standardized uptake value, *FDG-PET/CT* fluorodeoxyglucose-positron emission tomography/computed tomography, *SPECT* single-photon emission computed tomography

low, with 8 of 232 sites showing inter-observer mismatch in our study. Visual scoring is a step evaluation; therefore, the degree of uptake cannot be quantitatively evaluated. The SUV is a widely used quantitative index in PET imaging but has not been used in SPECT imaging. The lack of quantitative analysis is a major disadvantage of SRS compared with PET. In PET/CT, CT data is used for attenuation correction in the PET image to quantify the accumulation. Recently, SPECT/CT systems have been developed, and as with PET/CT, performing attenuation correction using CT data and quantifying the accumulation is now possible. The development of hybrid SPECT/CT scanners and quantitative SPECT analysis software has enabled the conversion of radioactivity into quantitative indices. The CT data derived from SPECT/

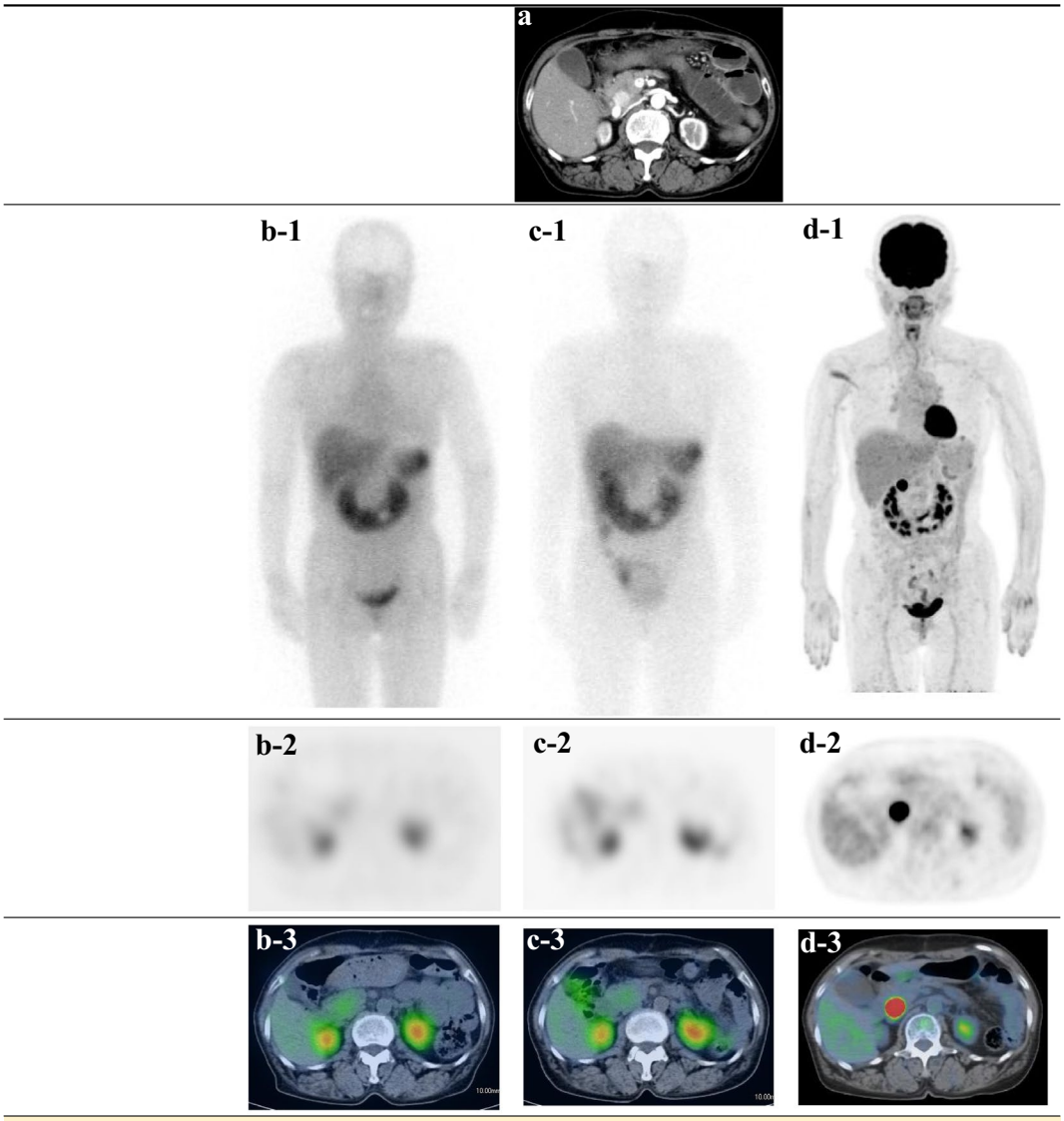

Visual score (SPECT)	3	4	—
SUVmax	3.4	2.5	57.3

Fig. 7 **a** Imaging findings of Patient 3 from the initial staging group. A grade 2 NET in the pancreatic head, measuring 1.7 cm, shows strong homogeneous enhancement in the early phase of dynamic CT. There is no evidence of lymph node or distant metastases on body CT and SRS. The primary lesion shows moderate uptake as follows: b-1 to b-3) score: 3, SUVmax: 3.4 in the early phase. c-1 to c-3) score: 4, SUVmax: 2.5 in the delayed phase. d-1 to d-3) intense FDG uptake with an SUVmax of 57.3 on FDG-PET/CT. *NET* neuroendocrine tumor, *CT* computed tomography, *SRS* somatostatin receptor scintigraphy, *SUVmax*: maximum standardized uptake value, *FDG-PET/CT* fluorodeoxyglucose-positron emission tomography/computed tomography, *SPECT* single-photon emission computed tomography

CT is used for attenuation correction and obtaining morphological information. Previously, we adapted the SUV and proposed new quantitative indices for dopamine-transporter SPECT with ^{123}I-ioflupane and cardiac amyloidosis scintigraphy with ^{99m}Tc-pyrophosphate [7, 8]. We thought of adapting a quantitative index, i.e., SUVmax, to SRS, giving it a new role in the management of patients with NEN. Quantitative FDG-PET indices such as the SUV, MTV, and TLG are routinely used in clinical practice. In SSTR-PET, quantitative evaluation with the SUV is possible, and a volumetric index, DTTV, is reportedly useful in determining treatment efficacy. Although SSTR-PET is preferred over SRS for molecular imaging of NETs due to its high spatial resolution and quantification, SRS remains important in NET imaging. We conducted this study believing that identifying a quantitative index for SRS, similar to those for FDG-PET and SSTR-PET, could be useful for patient management. SRS assessment is mainly performed visually

Table 6 Reduction score and reduction rate of primary and metastatic lesions of patients who underwent follow-up

	NET location	Grade	Therapy	Phase	Primary lesion			Liver metastasis			Lymph node metastasis			Bone metastasis		
					Reduction score		RR	Reduction score		RR	Reduction score		RR	Reduction score		RR
					Planar	SPECT		Planar	SPECT		Planar	SPECT		Planar	SPECT	
1	Pancreas	2	Chemo	4 h	–	–	–	–	–	–						
				24 h	–	–	–	–	–	–						
			Chemo	4 h	1	0	58%	n/a	− 2	− 691%						
				24 h	1	0	50%	n/a	− 2	− 771%						
			PRRT	4 h	0	1	59%	1	1	80%						
				24 h	0	1	62%	1	1	80%						
2	Pancreas	2	Chemo	4 h	–	–	–	–	–	–	–	–	–			
				24 h	–	–	–	–	–	–	–	–	–			
			Chemo	4 h	0	0	− 59%	0	0	− 186%	0	0	− 10%			
				24 h	0	0	− 95%	0	0	− 266%	0	0	− 26%			
			PRRT	4 h	n/a	3	96%	2	1	94%	n/a	n/a	96%			
				24 h	n/a	3	95%	2	1	95%	n/a	n/a	97%			
3	Pancreas	2	Chemo	4 h	–	–	–	–	–	–	–	–	–			
				24 h	–	–	–	–	–	–	–	–	–			
			Chemo	4 h	0	0	− 13%	− 1	− 1	− 119%	n/a	0	− 65%			
				24 h	0	0	− 57%	− 1	− 1	− 159%	n/a	0	− 115%			
4	Duodenum	2	Chemo	4 h	–	–	–	–	–	–	–	–	–	–	–	–
				24 h	–	–	–	–	–	–	–	–	–	–	–	–
			Chemo	4 h	n/a	0	− 85%	0	0	− 216%	0	0	− 21%	0	0	32%
				24 h	n/a	0	− 61%	0	0	− 249%	0	0	− 12%	0	0	31%
5	Duodenum	2	Chemo	4 h	–	–	–	–	–	–	–	–	–			
				24 h	–	–	–	–	–	–	–	–	–			
			Chemo	4 h	0	0	− 10%	0	0	− 9%	0	0	− 1%			
				24 h	0	0	− 60%	0	0	− 29%	0	0	− 53%			
6	Lung	2	Chemo	4 h	–	–	–	–	–	–	–	–	–	–	–	–
				24 h	–	–	–	–	–	–	–	–	–	–	–	–
			PRRT	4 h	1	2	51%	0	0	61%	2	2	44%	1	1	62%
				24 h	1	2	68%	0	0	70%	2	1	77%	1	1	75%

NET neuroendocrine tumor, *RR* reduction rate, *SPECT* single-photon emission computed tomography, *Chemo* chemotherapy, *PRRT* peptide receptor radionuclide therapy, *n/a* not applicable

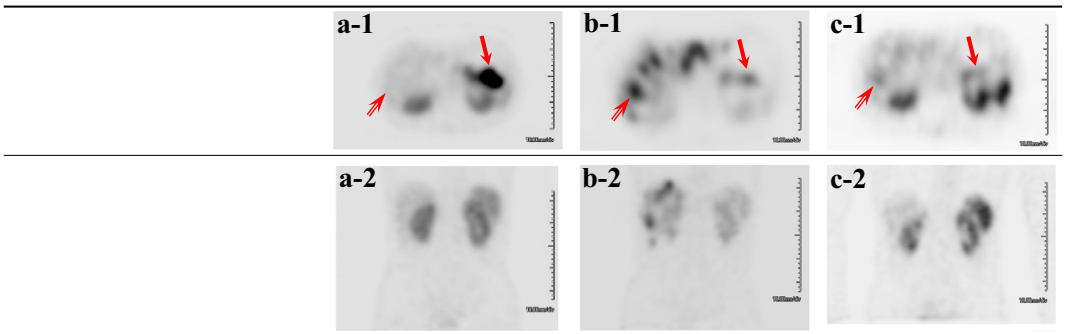

Visual score (SPECT)	**Primary**	5	5	4
	Meta	3	5	4
Reduction score	**Primary**	—	0	1
	Meta	—	-2	1
SUVmax	**Primary**	26.8	11.3	4.6
	Meta	2.5	19.5	4.0
Reduction rate	**Primary**	—	58 %	59 %
	Meta	—	-691 %	80 %
SUVmean, SUVmax	**Kidney**	5.6, 7.2	3.5, 4.9	3.9, 7.7
	Spleen	4.1, 4.9	2.7, 3.8	6.4, 10.4

Fig. 8 Imaging findings from the early phase (4 h) of Patient 1 from the follow-up group who had grade 2 NET of the pancreas with liver metastasis treated with chemotherapy and PRRT. **a** After the first chemotherapy course. **b** After the second chemotherapy course. **c** After PRRT. a-1) Primary lesion at the pancreatic tail shows very intense uptake, a visual score of 5, and an SUVmax of 26.8. The liver metastasis shows almost the same uptake as the liver, a visual score of 3, and an SUVmax of 2.5. b-1) The primary lesion uptake on SRS has considerably decreased. The visual score is 5, SUVmax is 11.3, the reduction score is 0, and the reduction rate is 58%. Multiple liver metastases can be identified, with a visual score of 5, an SUVmax of 19.5, a reduction score of − 2, and a reduction rate of − 691%. c-1) The primary lesion uptake on SRS has slightly decreased compared with that on the previous scan. The visual score is 4, SUVmax is 4.6, the reduction score is 1, and the reduction rate is 59%. Multiple liver metastases can be identified, with a visual score of 4, an SUVmax of 4.0, a reduction score of 1, and a reduction rate of 80%. a-2), b-2), and c-2) Coronal-view images of the liver, kidney, and spleen. The degree and pattern of physiological accumulation for the liver, kidney, and spleen vary among individuals. In a-2, the liver, spleen, and kidneys are highly accumulated. In b-2, the liver and kidneys are almost equally accumulated, and they show higher accumulation than the spleen. In c-2, the spleen is more accumulated than the kidneys. *NET*: neuroendocrine tumor, *PRRT* peptide receptor radionuclide therapy, *SUVmax* maximum standardized uptake value, *SRS* somatostatin receptor scintigraphy, *SPECT* single-photon emission computed tomography, *Meta* metastasis, *SUVmean* mean standardized uptake value

and entails a comparison of abnormal uptake in the lesion with physiological uptake in reference organs such as the liver, kidney, or spleen [6]. Herein, we first adapted the SUV to SRS and proposed a quantitative assessment method for both physiological and abnormal uptake. Besides analyzing abnormal uptake, we needed to quantify the physiological uptake. We established the range and mean of the physiological SUV of organs, including the liver, kidney, and spleen. The normal SUV varied over a range, which was the largest in the liver, followed by the kidney and spleen, respectively, and matched the visual score. Furthermore, physiological uptake tended to decline with the quantitative index from the early to the delayed phase, even if no difference between the dual-phase images could be visually noted. In contrast, the lesion SUV showed a variable pattern of increase or decrease, or no change, in the delayed phase of dual-phase imaging. The SUV range varied for each score, especially score 5. The degree of uptake can be evaluated in great detail when the lesion uptake is substantially higher than that of the kidney, the liver and kidney show almost equal uptake, or the liver shows more intense uptake than that of the kidney. By thus quantifying lesion accumulation, objective quantitative evaluation is possible regardless of the physiological accumulation. Analyzing the correlation among the SUV, pathological grade, and visual score revealed that all three patients with grade 1 NET had a visual score of 5 and the SUV ranges were 5.0–10.3 at 4 h and 2.5–9.1 at 24 h, and 7 patients with grade 2 lesions had visual scores of 3–5 (equal to or more than that of the liver), and the SUV range was wide. Even when the SUVmax changed slightly, the visual score did not change because visual scoring is a step scoring. We found that grade 1 lesions showed intense uptake, and grade 2 lesions showed moderate to intense uptake depending on pathological differentiation and tumor proliferation.

These results support those of previous studies [12]. We investigated the relationship between histopathologic differentiation and cell proliferative potential (histopathological grade) in patients with NET who had been diagnosed before treatment by combining conventional visual scoring and quantitative evaluation using SUV. All patients with grade 1 lesions had a visual score of 5, whereas some patients with grade 2 lesions had a score of 3 or 4. Comparing each patient's scores at 4 and 24 h revealed that all patients with grade 1 lesions had a score of 5 at both 4 and 24 h, whereas the score of one patient with a grade 2 lesion increased from 3 at 4 h to 4 at 24 h. Furthermore, SUV evaluation provided a detailed quantitative index of the change from the 4 h to the 24 h time point. The accumulation showed a wide range even when the score was the same. Patients with grade 2 lesions showed the highest SUV. We expect the correlation between pathological grade and SUV obtained using SRS to become clearer with the collection of more cases in the future. Additionally, predicting the pathological grade based on the accumulation pattern may become possible due to the time-phase difference. Some participants underwent two examinations with SRS and FDG-PET/CT. One patient with grade 1 P-NET showed intense uptake with a visual score of 5, an SUVmax of 5.0 (4 h) and 2.5 (24 h) on SRS, and an SUVmax of 1.9 on FDG-PET/CT, which closely approximated that of the pancreas. A patient with grade 2 P-NET showed moderate uptake, a score of 3, and an SUVmax of 3.4 in the early phase; a visual score of 4 and an SUVmax of 2.5 in the delayed phase; and very intense uptake with an SUVmax of 57.3 on FDG-PET/CT. Thus, grade 2 NET lesions can demonstrate highly intense uptake according to tumor activity, i.e., proliferation. By comparing the quantitative methods, including SUV, established for SSTR-PET and FDG-PET [13, 14], with SRS-SUV, the relationship with cell proliferation, mitosis, and pathological grade can be elucidated.

The PET Response Criteria In Solid Tumors (PERCIST), which builds upon the Response Evaluation Criteria in Solid Tumors (RECIST) used to determine the therapeutic efficacy of tumors, was established in 2009 and is widely used in clinical practice [15–17]. The RECIST refers to the lesion status obtained from imaging studies but does not include SPECT [18, 19]. Predicting the therapeutic effect of SPECT is difficult due to the low spatial resolution and lack of quantitative indices. The response to PRRT has been previously predicted with the Krenning score, metastasis to liver uptake ratio (M/L ratio), and asphericity [20–22]. Christoph et al. reported that asphericity is a more effective predictive parameter for PRRT in patients with gastroenteropancreatic NEN than the Krenning score and M/L ratio [22]. Herein, we devised a quantitative analysis method by applying the SUV derived from PET to ^{111}In-pentetreotide SRS, enabling quantitative assessment of individual lesions and monitoring the therapeutic effect using SUV in SRS. We calculated the reduction rate to reflect the response to treatment such as chemotherapy and PRRT. European guidelines recommend using SRS to determine the effectiveness of PRRT, and by quantitatively comparing the lesion accumulation (SUV) on SRS before and after PRRT, SRS can be considered equivalent to PET [23]. We compared the reduction rate derived from the SUVmax of SRS before and after treatment with the reduction score derived from the visual score. Even when the reduction score is 0, the reduction rate can reflect changes in accumulation, and the treatment effect can be quantitatively analyzed. One drawback of visual evaluation is that it is assessed subjectively based on the physiological accumulation in the liver, kidney, and spleen. For example, in one patient in the follow-up group, the SUV mean of the kidneys and spleen significantly changed from 3.5–5.6 to 2.7–6.4 from the first to the third examination, and the SUVmax was 4.9–7.7 and 3.8–10.4, respectively. Since physiological accumulation is not constant, correctly evaluating the treatment effect via visual evaluation of physiological accumulation is difficult. However, quantitative analysis using SUV is not affected by physiological accumulation. SUV may find application as a new imaging biomarker for initial staging and restaging. Combining quantitative evaluation using SUV with conventional visual evaluation makes it possible to clarify the relationship between the magnitude of each degree of integration and to make an objective assessment. In a study comparing the detection sensitivity of SRS and FDG-PET with respect to the Ki67 index, the sensitivities of SRS and FDG-PET were 87% and 41%, respectively, for a Ki67 index < 2; 96% and 73%, respectively, for a Ki67 index of 2–15; and 69% and 92%, respectively, for a Ki67 index > 15. SRS is reportedly useful for well-differentiated NETs, and FDG-PET for high-grade NETs [24, 25]. ^{68}Ga-labeled PET can demonstrate SSTR expression with high image quality and detectability that is superior to that of SRS [26]. Ortega et al. reported multiple quantitative indices for SSTR-PET/CT to predict the response to PRRT [27]. Clinicians prefer SSTR-PET over SRS due to its higher spatial resolution and anomaly detectability, as well as its quantitative evaluation capability. Buchmann et al. compared ^{68}Ga-DOTATOC and ^{111}In-pentetotide using radiation counts and SUVs to calculate the tumor proportion and physiological accumulation [26]. However, since the equations used for the two indicators differ, simply comparing the accumulation of ^{111}In and ^{68}Ga is impossible. Thomas et al. did not compare lesion accumulation between ^{111}In-pentetreotide and ^{68}Ga-DOTATATE, because SRS cannot be quantitatively analyzed [28]. Using the SRS-SUV, examining the relationship between the two examinations may be possible. Nevertheless, ^{68}Ga-labeled PET is not widely used because of limitations associated with radioisotope production and supply,

although its use enables quantitative evaluation similar to PET using SRS in facilities where SSTR-PET is unavailable.

There are two limitations of this study. The first is the small sample size. This study was performed at a single center using only one hybrid SPECT/CT system; the patient population was small, and no patients with grade 3 NETs or NECs were included. Five patients with P-NET from the initial staging group did not undergo pathological confirmation. The second limitation is that the BCF differs according to the SPECT/CT system. However, this quantitative analysis method can be performed anywhere, and the BCF must be calculated for each SPECT/CT system according to the clinical scan protocol and parameters used at each institution. The SUV may differ for each imaging system. Future studies should focus on clarification and standardization of the quantitative index for different SPECT/CT systems.

Conclusion

We adapted the SUV to SRS and established the SUV range for physiological uptake in the liver, kidney, and spleen. SRS remains important in NET management. SRS-SUV is a potential novel tumor marker for primary and metastatic NET. A combination of quantitative assessment using SRS-SUV with simple conventional visual scoring can enable objective and quantitative assessment of the degree of and temporal changes in accumulation.

Acknowledgements We would like to thank Editage (www.editage.com) for English language editing. We are deeply grateful to everyone involved in this study. This research received no external funding.

Author contributions HO conceived the idea of the study. YU performed clinical data analysis and drafted this paper. HO and YO interpreted the planar and SPECT images, respectively. TO, DI, SA, and YK performed the phantom experiment and clinical nuclear medicine examination with technical advice. RK provided advice on the preparation of this article. TB and NM performed the phantom experiment. YO and TT performed clinical diagnosis and suggestion of neuroendocrine tumor pathologies. MH provided clinical suggestions. All authors have read and agreed to the published version of the manuscript.

Funding This research received no external funding.

Data Availability The data that support the findings of this study are available on request from the corresponding author (HO). The data are not publicly available since they contain information that could compromise the privacy of the research participants.

Declarations

Conflict of interest The authors declare no conflict of interest.

Ethical approval The study was approved by the Institutional Ethics Committee of Tokushima University Hospital (approval number: 4173).

Informed consent The requirement of written informed consent was waived by the Institutional Ethics Committee owing to the retrospective study design.

References

1. Ito T, Masui T, Komoto I, Doi R, Osamura RY, Sakurai A, et al. JNETS clinical practice guidelines for gastroenteropancreatic neuroendocrine neoplasms: diagnosis, treatment, and follow-up: a synopsis. J Gastroenterol. 2021;56:1033–44.
2. Dasari A, Shen C, Halperin D, Zhao B, Zhou S, Xu Y, et al. Trends in the incidence, prevalence, and survival outcomes in patients with neuroendocrine tumors in the United States. JAMA Oncol. 2017;3:1335–42.
3. Wang R, Zheng-Pywell R, Chen HA, Bibb JA, Chen H, Rose JB. Management of gastrointestinal neuroendocrine tumors. Clin Med Insights Endocrinol Diabetes. 2019;12:1179551419884058.
4. Baumann T, Rottenburger C, Nicolas G, Wild D. Gastroenteropancreatic neuroendocrine tumours (GEP-NET) - imaging and staging. Best Pract Res Clin Endocrinol Metab. 2016;30:45–57.
5. Mikołajczak R, Maecke HR. Radiopharmaceuticals for somatostatin receptor imaging. Nucl Med Rev Cent East Eur. 2016;19:126–32.
6. Krenning EP, Valkema R, Kooij PP, Breeman WA, Bakker WH, deHerder WW, et al. Scintigraphy and radionuclide therapy with [indium-111-labelled-diethyl triamine penta-acetic acid-D-Phe1]-octreotide. Ital J Gastroenterol Hepatol. 1999;31:S219–23.
7. Bando R, Otsuka H, Otani T, Matsuda N, Azane S, Kunikane Y, et al. A new quantitative index in the diagnosis of Parkinson syndrome by dopamine transporter single-photon emission computed tomography. Ann Nucl Med. 2021;35:504–13.
8. Matsuda N, Otsuka H, Otani T, Azane S, Kunikane Y, Otomi Y, et al. New quantitative indices of cardiac amyloidosis with 99mTc-pyrophosphate scintigraphy. Jpn J Radiol. 2023;41:428–36.
9. Schillaci O, Spanu A, Scopinaro F, Falchi A, Danieli R, Marongiu P, et al. Somatostatin receptor scintigraphy in liver metastasis detection from gastroenteropancreatic neuroendocrine tumors. J Nucl Med. 2003;44:359–68.
10. Dillon JS. Workup of gastroenteropancreatic neuroendocrine tumors. Surg Oncol Clin N Am. 2020;29:165–83.
11. Kubota K, Okasaki M, Minamimoto R, Miyata Y, Morooka M, Nakajima K, et al. Lesion-based analysis of (18)F-FDG uptake and (111)In-Pentetreotide uptake by neuroendocrine tumors. Ann Nucl Med. 2014;28:1004–10.
12. Chougnet CN, Leboulleux S, Caramella C, Lumbroso J, Borget I, Déandreis D, et al. Frequency and characterization of gastro-entero-pancreatic neuroendocrine tumor patients with high-grade of uptake at somatostatin receptor scintigraphy. Endocr Relat Cancer. 2013;20:229–39.
13. Weber M, Telli T, Kersting D, Seifert R. Prognostic implications of PET-derived tumor volume and uptake in patients with neuroendocrine tumors. Cancers (Basel). 2023;15:3581.
14. Sanli Y, Garg I, Kandathil A, Kendi T, Zanetti MJB, Kuyumcu S, et al. Neuroendocrine tumor diagnosis and management: ^{68}Ga-DOTATATE PET/CT. AJR Am J Roentgenol. 2018;211:267–77.
15. Wahl RL, Jacene H, Kasamon Y, Lodge MA. From RECIST to PERCIST: evolving Considerations for PET response criteria in solid tumors. J Nucl Med. 2009;50:122S-S150.
16. Jh O, Lodge MA, Wahl RL. Practical PERCIST: a simplified guide to PET response criteria in solid tumors 1.0. Radiology. 2016;280:576–84.

17. Martínez A, Infante JR, Quirós J, Rayo JI, Serrano J, Jiménez P, et al. Prognostic value of PERCIST and PET/CT metabolic parameters after neoadjuvant treatment in patients with esophageal cancer. Rev Esp Med Nucl Imagen Mol (Engl Ed). 2022;41:360–7.
18. Eisenhauer EA, Therasse P, Bogaerts J, Schwartz LH, Sargent D, Ford R, et al. New response evaluation criteria in solid tumours: revised RECIST guideline version 1.1. Eur J Cancer. 2009;45:228–47.
19. Ko CC, Yeh LR, Kuo YT, Chen JH. Imaging biomarkers for evaluating tumor response: RECIST and beyond. Biomark Res. 2021;9:52.
20. Hofman MS, Lau WF, Hicks RJ. Somatostatin receptor imaging with 68ga DOTATATE PET/CT: clinical utility, normal patterns, pearls, and pitfalls in interpretation. Radiographics. 2015;35:500–16.
21. Kratochwil C, Stefanova M, Mavriopoulou E, Holland-Letz T, Dimitrakopoulou-Strauss A, Afshar-Oromieh A, et al. SUV of [68ga]DOTATOC-PET/CT predicts response probability of PRRT in neuroendocrine tumors. Mol Imaging Biol. 2015;17:313–8.
22. Wetz C, Apostolova I, Steffen IG, Hofheinz F, Furth C, Kupitz D, et al. Predictive value of asphericity in pretherapeutic [111In] DTPA-octreotide SPECT/CT for response to peptide receptor radionuclide therapy with [177Lu]DOTATATE. Mol Imaging Biol. 2017;19:437–45.
23. Hicks RJ, Kwekkeboom DJ, Krenning E, Bodei L, Grozinsky-Glasberg S, Arnold R, et al. ENETS consensus guidelines for the standards of care in neuroendocrine neoplasia: peptide receptor radionuclide therapy with radiolabeled somatostatin analogues. Neuroendocrinology. 2017;105:295–309.
24. Binderup T, Knigge U, Loft A, Mortensen J, Pfeifer A, Federspiel B, et al. Functional imaging of neuroendocrine tumors: a head-to-head comparison of somatostatin receptor scintigraphy, 123I-MIBG scintigraphy, and 18F-FDG PET. J Nucl Med. 2010;51:704–12.
25. Squires MH 3rd, Volkan Adsay N, Schuster DM, Russell MC, Cardona K, Delman KA, et al. Octreoscan versus FDG-PET for neuroendocrine tumor staging: a biological approach. Ann Surg Oncol. 2015;22:2295–301.
26. Buchmann I, Henze M, Engelbrecht S, Eisenhut M, Runz A, Schäfer M, et al. Comparison of 68ga-DOTATOC PET and 111In-DTPAOC (Octreoscan) SPECT in patients with neuroendocrine tumours. Eur J Nucl Med Mol Imaging. 2007;34:1617–26.
27. Ortega C, Wong RKS, Schaefferkoetter J, Veit-Haibach P, Myrehaug S, Juergens R, et al. Quantitative ^{68}Ga-DOTATATE PET/CT parameters for the prediction of therapy response in patients with progressive metastatic neuroendocrine tumors treated with ^{177}Lu-DOTATATE. J Nucl Med. 2021;62:1406–14.
28. Hope TA, Calais J, Zhang L, Dieckmann W, Millo C. 111In-pentetreotide scintigraphy versus 68Ga-DOTATATE PET: impact on Krenning scores and effect of tumor burden. J Nucl Med. 2019;60:1266–9.